# Neutron Capture Reactions near $N = 82$ Shell-closure

Saumi Dutta,* Dipti Chakraborty,† G. Gangopadhyay,‡ and Abhijit Bhattacharyya§
*Department of Physics, University of Calcutta*
*92, Acharya Prafulla Chandra Road,*
*Kolkata-700 009, India*

Neutron capture cross-sections have been calculated in nuclei near the $N = 82$ neutron shell closure. These nuclei are of astrophysical interest, participating in s-process and p-process. A semi-microscopic optical model have been used with the potential being obtained through folding the target density with the DDM3Y nucleon nucleon interaction. Theoretical density values have been calculated in the relativistic mean field approach. The calculated cross-section, as a function of neutron energy, agree reasonably well with experimental measurements. Maxwellian averaged cross-sections, important for astrophysical processes, have been calculated.



## I. INTRODUCTION

After the seminal work of Burbidge *et al.* [1], the method of creation of heavy elements through the slow neutron capture or s-process has been firmly established. A recent review that discusses our current understanding of the s-process may be found in Käppeler *et al.* [2] It is now understood that a major fraction of the nuclear abundance in the mass region $90 < A < 209$ is due to the main s-process which takes place in He shells in low-mass AGB stars of moderate mass.

The role of the neutron capture reaction in s-process has been explored in many works. More accurate measurements have shown the inadequacy of the classical site-independent s-process and have paved the way to coupling with stellar models. A mass region, where the reaction cross-section plays a very important role, lies near the $N = 82$ shell closure. Here, the elements Ba ($Z = 56$) to Sm ($Z = 62$) have small cross-sections for neutron capture reactions because of the proximity of the shell-closure. Hence, they act as bottle-necks for the s-process reaction path. An s-process peak occurs at $^{138}$Ba. There are several s-only nuclides such as $^{134,136}$Ba, $^{142}$Nd, and $^{148,150}$Sm in this mass region. In the case of pairs of s-only isotopes such as $^{134,136}$Ba, the cross-sections and the abundances can be used to obtain the branching ratios of the s-process. Nuclei on the s-process path that have comparable beta decay rates and neutron capture rates act as branch points as the nucleosynthesis path bifurcates towards both the proton and neutron rich sides while passing through them. The cross-sections at the branch points and s-only isotopes can provide important clues to the physical environments where the s-process takes place.

Although experimental measurements are available for many isotopes in the mass region, cross-section values are required for some unstable nuclei important to determine the branching ratios. Such nuclei include $^{134,135}$Cs, $^{141}$Ce, $^{147}$Nd, and $^{147,148}$Pm. We should also remember that although the classical or canonical s-process calculations use the Maxwellian averaged cross-sections (MACS) at a single thermal energy ($\approx 30$ keV usually), recent approaches, which couple stellar models with the s-process network, need MACS at different thermal energies. Measurements are not always available and extrapolation to too distant value from the measured ones may lead to errors. Theoretical calculations can supplement the experimental measurements in this regard.

There are some neutron capture reactions in this mass region whose studies are relevant for the astrophysical p-process. Photodissociation reactions such as $(\gamma, n)$ occur in extremely hot environments. Explosively burning Ne/O layer in core-collapse supernovae heated by the outgoing shock-wave may provide such an environment. Cross section values are very important as various photo-dissociation reactions such as $(\gamma, n)$, $(\gamma, p)$ and $(\gamma, \alpha)$ compete at high temperature. The emitted neutrons also may be absorbed after the shock wave passes through the layer. Thus it is very important to measure the cross-sections for relevant $(\gamma, n)$ reactions at thermal energies. The reverse process, i.e., $(n, \gamma)$ reactions may serve the purpose. For example, Dillmann *et al.* [3] studied a number of $(n, \gamma)$ reactions with neutrons from the $^7$Li$(p, n)^7$Be reaction to simulate a Maxwellian neutron

*Electronic address: saumidutta89@gmail.com
†Electronic address: diptichakraborty2009@gmail.com
‡Electronic address: ggphy@caluniv.ac.in
§Electronic address: abhattacharyyacu@gmail.com

distribution at 25 keV thermal energy.

Neutron capture reactions have been studied in various methods. Older experiments usually used neutron beams of comparatively wide resolution. As the resonances in this region are narrow (less than 1 eV), one gets an average cross-section in such experiments. Extremely high resolution experiments using the neutron time of flight technique (TOF) have been used to study the resonances. However, we are more interested in the Maxwellian averaged cross-sections. In such cases, the data have been compressed into coarse energy bins to obtain MACS values. In some other experiments, sources of neutrons have been used that closely simulated the thermal neutron spectrum at certain temperatures. They can provide direct measurement of MACS values.

In the present work, we have studied low energy neutron capture cross-sections of the nuclei near $N = 82$. In the next section, we briefly present our formalism. In Section III, we discuss our results for important neutron capture reactions near $N = 82$ shell closure, first at various neutron energies and compare with experimental measurements. It is followed by a calculation of the MACS values, first at 30 keV, and later at different thermal energies for some selected isotopes. Finally we summarize our work.

## II. CALCULATION

We have used a semi-microscopic procedure to calculate the neutron capture cross-section in the present work. This method has been followed in a number of our recent works [4–9]. For example, in Chakraborty *et al.* [9], this procedure has been utilized to study proton capture reactions, important for the astrophysical p-process in mass $110-125$ region. In the present approach, we extend it to study neutron capture reactions near $N = 82$ shell closure.

To briefly describe our procedure, we have assumed spherical symmetry for the target nuclei. The density profiles of the nuclei have been calculated in co-ordinate space in the relativistic mean field (RMF) approach using the FSU Gold Lagrangian density [10]. The charge density is obtained from the point proton density considering the finite size of the proton using a standard Gaussian form factor $F(r)$ [11] as follows.

$$\rho(r) = e \int \rho(\mathbf{r\prime}) F(\mathbf{r} - \mathbf{r\prime}) d\mathbf{r\prime} \quad (1)$$

$$F(r) = (a\sqrt{\pi})^{-3} exp(-r^2/a^2) \quad (2)$$

with $a = \sqrt{2/3}a_p$, where $a_p = 0.80$ fm is the root mean square (r.m.s.) charge radius of the proton. The charge density thus obtained is used to calculate r.m.s charge radii for some nuclei in and around the concerned region of shell closure to compare with experimentally available values. Comparison with measured values serves as a check on the applicability and reliability of the Lagrangian density used in the calculations.

The nuclear density has then been folded with the DDM3Y nucleon-nucleon interaction to obtain the optical model potential. The interaction at distance $r$ for density $\rho$ and projectile energy in centre of mass frame $E$, supplemented by a zero range pseudo-potential, is given by

$$v(r, \rho, E) = t^{M3Y}(r, E) g(\rho) \quad (3)$$

with the M3Y interaction [12, 13] in MeV

$$t^{M3Y} = 7999\frac{e^{-4r}}{4r} - 2134\frac{e^{-2.5r}}{2.5r} - 276(1 - \frac{E}{200A})\delta(r) \quad (4)$$

Here $E$ is given in MeV, $r$ in fm and $A$ is the mass number of the projectile. The density dependent factor is [14]

$$g(\rho) = C(1 - \beta\rho^{2/3}) \quad (5)$$

with $C$ and $\beta$ taking values 2.07 and $1.624 fm^2$, respectively, obtained from nuclear matter calculation [15]. We also use an additional spin-orbit potential $U^{so}_{n(p)}(r)$ with energy dependent phenomenological potential depths $\lambda_{vso}$ and $\lambda_{wso}$ according to Scheerbaum prescription [16], given by

$$U^{so}_{n(p)}(r) = (\lambda_{vso} + i\lambda_{wso})\frac{1}{r}\frac{d}{dr}(\frac{2}{3}\rho_{p(n)} + \frac{1}{3}\rho_{n(p)}) \quad (6)$$

with,

$$\lambda_{vso} = 130 exp(-0.013E) + 40 \quad (7)$$

$$\lambda_{wso} = -0.2(E - 20) \quad (8)$$

The DDM3Y interaction provides only the real part of the potential. The imaginary part of the potential is taken to be identical with the real part. This optical model potential has been used to study the neutron capture reaction cross-sections.

The computer code TALYS1.6 [17] has been used for cross-section calculations. Microscopic level densities,

which are important ingredients in statistical model calculations of reaction cross-sections, are taken from the calculations of Goriely included in the code. The $\gamma$-strength functions for the dominant E1 $\gamma$ transitions, are taken from Goriely's hybrid model [18]. Width fluctuation corrections in compound nuclear decay are also considered. These are especially important near threshold energy of new channel openings where channel strengths differ significantly. Radial densities are taken from RMF calculations. Pairing energy correction has also been included. At low incident energies, *i.e.* below a few MeV, mainly binary reactions occur and very often the target and compound nuclei only are involved in the whole reaction chain. A maximum of 30 discrete levels are taken for both target nuclei and residual nuclei. Hauser-Feshbach calculations are performed with full $j, l$ coupling. All these options are included in TALYS code.

## III. RESULTS

### A. Results of RMF calculations

The most important RMF result relevant to the calculation of neutron capture in the present formalism is the density profile. Experimental results on density are available for three nuclei with $N = 82$, *viz.* $^{138}$Ba, $^{142}$Nd, and $^{144}$Sm. In Fig. 1, we plot the charge density obtained in our calculation for these three nuclei. The experimental densities for $^{138}$Ba and $^{142}$Nd have been generated from the parameters for a three parameter Gaussian function fitted to describe the electron scattering data of Heisenberg *et al.* [19] For $^{144}$Sm, the Fourier-Bessel coefficients obtained from fitting the experimental results of Moinester *et al.* [20] have been used.

Charge radius values, as a first moment of the charge distribution, can be compared with calculated results to check the success of theoretical approach. In Table I, we compare the calculated r.m.s. charge radius values with experimental data. From the comparison between experimental and calculated charge density and radius values, one can infer that the present RMF calculation can describe the nuclear density near $N = 82$ shell closure very well. We now employ the theoretical density values to derive the optical model potential and extract cross-sections for neutron capture.

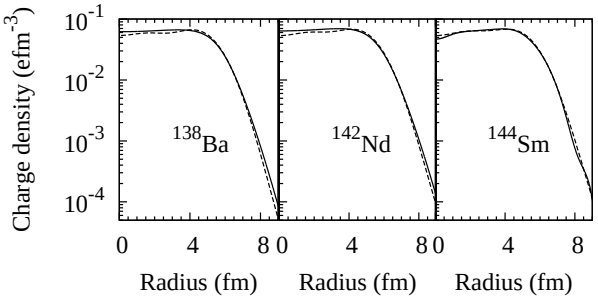


FIG. 1: Charge density in several $N = 82$ nuclei. Solid lines denote the model values using the parameters obtained from fitting the experimental data. Dashed lines indicate our results.

TABLE I: Charge radii of the nuclei studied in the present work. Experimental charge radii values are from the compilation of Angeli [21].

| Nucleus | $r_c$(fm) | | Nucleus | $r_c$(fm) | |
|---|---|---|---|---|---|
| | Exp. | Pres. | | Exp. | Pres. |
| $^{133}$Cs | 4.804 | 4.801 | $^{134}$Cs | 4.803 | 4.807 |
| $^{135}$Cs | 4.807 | 4.813 | $^{136}$Cs | 4.806 | 4.819 |
| $^{137}$Cs | 4.813 | 4.825 | | | |
| $^{130}$Ba | 4.829 | 4.797 | $^{132}$Ba | 4.831 | 4.808 |
| $^{134}$Ba | 4.830 | 4.820 | $^{135}$Ba | 4.827 | 4.826 |
| $^{136}$Ba | 4.833 | 4.832 | $^{137}$Ba | 4.833 | 4.837 |
| $^{138}$Ba | 4.838 | 4.843 | | | |
| $^{138}$La | 4.846 | 4.856 | $^{139}$La | 4.855 | 4.862 |
| $^{136}$Ce | 4.874 | 4.858 | $^{138}$Ce | 4.873 | 4.869 |
| $^{140}$Ce | 4.877 | 4.879 | $^{141}$Ce | | 4.892 |
| $^{142}$Ce | 4.906 | 4.905 | | | |
| $^{141}$Pr | 4.892 | 4.898 | $^{142}$Pr | | 4.910 |
| $^{143}$Pr | | 4.922 | | | |
| $^{142}$Nd | 4.912 | 4.915 | $^{143}$Nd | 4.923 | 4.927 |
| $^{144}$Nd | 4.944 | 4.939 | $^{145}$Nd | 4.958 | 4.953 |
| $^{146}$Nd | 4.975 | 4.965 | $^{147}$Nd | 4.984 | 4.977 |
| $^{147}$Pm | | 4.981 | $^{148}$Pm | | 4.993 |
| $^{144}$Sm | 4.944 | 4.950 | $^{147}$Sm | 4.984 | 4.985 |
| $^{148}$Sm | 5.001 | 4.998 | $^{149}$Sm | 5.011 | 5.010 |

### B. Cross-sections at various neutron energies

TALYS-1.6 is meant for analysis of data above the resolved resonance range, which is approximately 1 keV. We have compared the neutron capture cross-sections

with those experimental measurements which do not show resolved resonances at low energy.

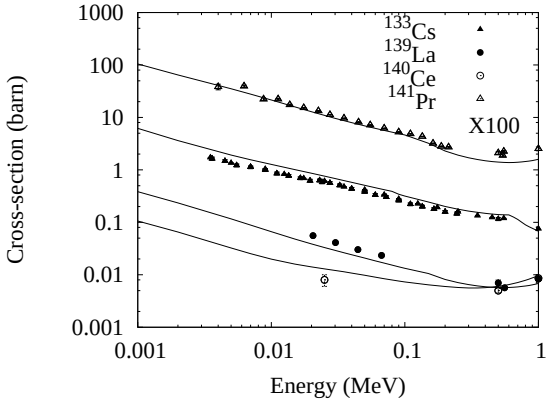


FIG. 2: Comparison of results of the present calculation with experimental measurements for $^{133}$Cs, $^{139}$La, $^{140}$Ce, and $^{141}$Pr. The solid lines indicate the theoretical results. For convenience, cross-section values for $^{141}$Pr have been multiplied by a factor of 100.

Theoretical neutron capture cross-section results for different neutron energy values have been compared with experiments in Figs. 2 - 5. In general, we have considered the more recent results. Our main interest lies in the nuclei which are important for astrophysical s- and p-processes. We generally present only those results where reasonable amount of experimental data exist for comparison. The exceptions are $^{139}$La and $^{140}$Ce because these three nuclei correspond to the $N = 82$ shell closure.

For convenience, we present the results for the elements, where only one isotope have been studied, in Fig. 2. These include $^{133}$Cs, $^{139}$La, $^{140}$Ce, and $^{141}$Pr. Experimental cross-section values for $^{133}$Cs$(n, \gamma)$ reaction are from Refs. [22–24]. The cross-section values are averaged over neutron energy range as the resonances are unresolved. For example, Yamamuro *et al.* [23] used the neutron beam from a tantalum photo-neutron source. They then average the cross-section over appropriate energy interval. For $^{139}$La, the data are from Refs. [24, 25]. Similarly, here also the neutron energy has a 5% error and we get an average value for various energies. Harnood *et al.* measured the neutron capture cross-section of $^{140}$Ce and $^{141}$Pr using the neutron TOF technique [26]. Voss *et al.* [27] also measured the cross-section for $^{141}$Pr in the range 3 to 225 keV. They also calculated the MACS values from their results. Voignier *et al.* also measured the capture cross-section in the energy range 0.5 to 3 MeV [28].

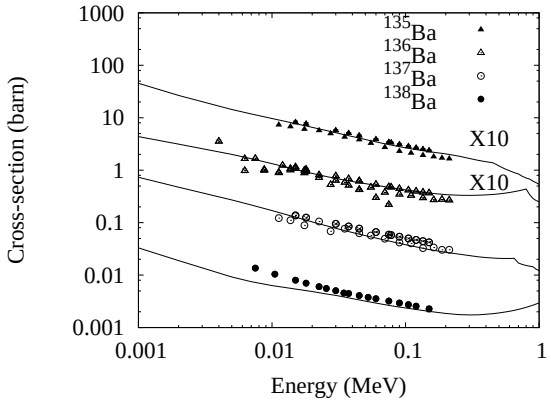


FIG. 3: Comparison of results of the present calculation with experimental measurements for $^{135-138}$Ba. The solid lines indicate the theoretical results. For convenience, cross-section values for $^{135,136}$Ba have been multiplied by a factor of 10.

In Fig. 3, we show the average neutron capture cross-sections in $^{135-138}$Ba nuclei and compare with experimental values between 1 keV and 1 MeV. Experimental cross-section values are from Refs. [29–32]. Voss *et al.* studied the neutron capture cross-section for $^{134-137}$Ba nuclei in the energy range from 3 to 225 keV using gold as a standard [29, 30]. Neutron capture by the neutron closed shell nucleus $^{138}$Ba has been studied in Refs. [31, 32].

Results for neutron capture cross-sections of $^{142-146}$Nd are shown in Fig. 4. Wisshak *et al.* [33, 34] studied the resonances above 3 keV in $^{142-146,148}$Nd. The data were then compressed in coarse bins to get the average behaviour. In another work, Veerapaspong *et al.* studied the neutron capture cross-sections for $^{143.145,146}$Nd [35]. Their data were put in a large energy bin of 10 keV wide. Their results agree with Refs. [33, 34] and our results though we have not shown the data in the figure.

In Fig. 5, we plot the experimental and calculated values for $^{144,147,148}$Sm. For $^{144}$Sm, experimental values are from Macklin *et al.* [36] where the authors have made measurements from 0.5 eV to 500 keV and have obtained the resonance parameters up to 100 keV. Wisshak *et al.* studied the neutron capture cross-section of $^{147-150,152}$Sm in the energy range 3 to 225 keV using gold as standard [37]. Mizumoto [38] measured the neutron capture cross-sections of $^{147,149}$Sm in the energy range

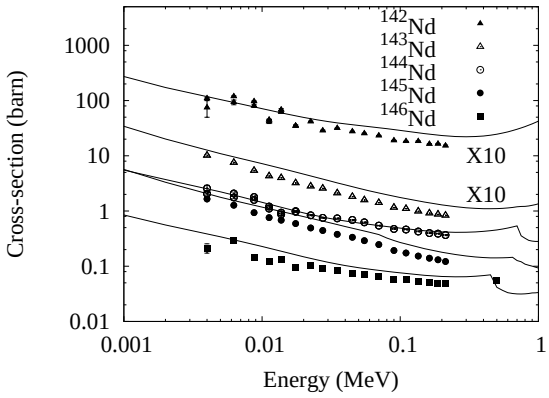


FIG. 4: Comparison of results of the present calculation with experimental measurements for $^{142-146}$Nd. The solid lines indicate the theoretical results. For convenience, cross-section values for $^{143,144}$Nd have been multiplied by a factor of 10.

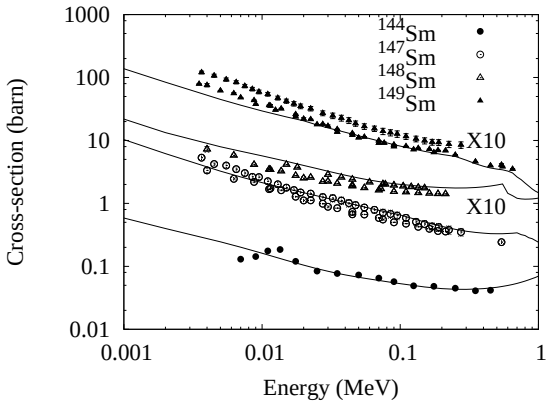


FIG. 5: Comparison of results of the present calculation with experimental measurements for $^{144,147-149}$Sm. The solid lines indicate the theoretical results. For convenience, cross-section values for $^{148,149}$Sm have been multiplied by a factor of 10.

3 - 300 keV using TOF technique. Diamet *et al.* used a similar technique to study $^{147-150,152,154}$Sm in the energy range 10 to 90 keV [39].

From Figs. 2 - 5, one can see that the theoretical calculation reproduces the experimental values in most of the cases. In the next subsection, we employ our method to calculate the MACS for some astrophysically important nuclei.

### C. Maxwellian averaged cross-sections

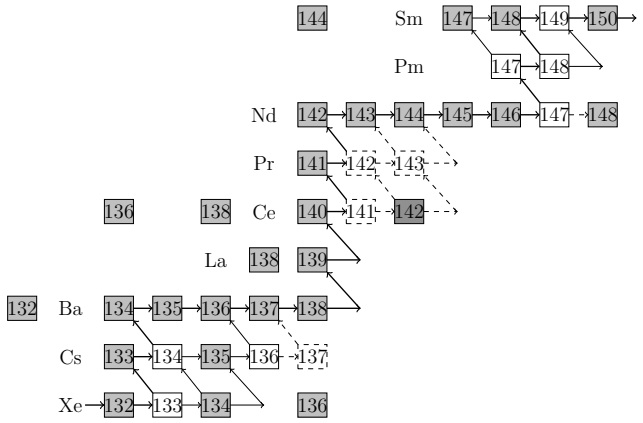


FIG. 6: The s-process path near the shell closure at $N = 82$. Also shown are some of the p-nuclei. See text for more details.

Apart from the nuclei with $N = 82$ in the s-process path, *i.e.* $^{138}$Ba, $^{139}$La, $^{140}$Ce, $^{141}$Pr, and $^{142}$Nd, which act as bottlenecks due to low cross-sections, neutron capture reactions in some other nuclei in the neighbourhood are also important for nucleosynthesis. In Fig. 6, we show the s-process path in the neighbourhood of the shell closure at $N = 82$. The shaded rectangles indicate stable and extremely long-lived nuclei. The weak branch points are indicated by rectangles with dashed lines. Similarly, weak s-process paths are indicated by dashed lines. One can see that there are strong branch points in the s-process path at $^{134}$Cs, $^{147}$Nd, and $^{147,148}$Pm. Besides, there are weaker branch points at $^{136}$Cs, $^{141}$Ce, and $^{147,149}$Pm. As already pointed out, the nuclei $^{134,136}$Ba, $^{142}$Nd, and $^{148,150}$Sm are s-only. There are several p-nuclei such as $^{130}$Ba (not shown in Fig. 6) $^{132}$Ba, $^{138}$La, $^{136,138}$Ce, and $^{144}$Sm, the last corresponding to the shell closure.

In Table II, we present the theoretically calculated MACS values at $kT = 30$ keV for a number of selected isotopes and compare with experimental measurements whenever available. Experimental values are from the database[40], which is an updated version of the compilation of Bao *et al.* [41]. Theoretical values from MOST calculation [42, 43], which are listed on the KADONIS online database, are also presented. MOST is a Hauser-Feshbach code which derives all nuclear inputs from global microscopic models. As one can see, agreement of our results with experiment is better than the

TABLE II: Maxwellian averaged cross-sections at $kT = 30$ keV for nuclei near the $N = 82$ shell closure. Experimental values are from Ref. [40]. See text for other experimental values. The nuclei with $N = 82$ are in bold font.

| | MACS(mb) | | | | MACS(mb) | | |
|---|---|---|---|---|---|---|---|
| Nucleus | Pres. | Exp. | MOST | Nucleus | Present | Exp. | MOST |
| $^{133}_{55}$Cs | 685 | 509±21 | 469 | $^{134}_{55}$Cs | 786 | | 805 |
| $^{135}_{55}$Cs | 147 | 160±10 | 148 | $^{136}_{55}$Cs | 90.4 | | |
| $^{137}_{55}$**Cs** | 16.1 | | | | | | |
| $^{130}_{56}$Ba | 625.2 | 746±34 | 490 | $^{132}_{56}$Ba | 393 | 397±16 | 227 |
| $^{134}_{56}$Ba | 158 | 176.0± 5.6 | 117 | $^{135}_{56}$Ba | 528 | 455± 15 | 259 |
| $^{136}_{56}$Ba | 74.6 | 61.2±2.0 | 49.4 | $^{137}_{56}$Ba | 81.8 | 76.3±2.4 | 95.4 |
| $^{138}_{56}$**Ba** | 4.14 | 4.00±0.20 | 2.79 | | | | |
| $^{138}_{57}$La | 417 | | 337 | $^{139}_{57}$**La** | 31.0 | 32.4±3.1 | 45.9 |
| $^{136}_{58}$Ce | 547 | 328±21 | 206 | $^{138}_{58}$Ce | 137 | 179±5 | 60.5 |
| $^{140}_{58}$**Ce** | 12.7 | 11.0±0.4 | 6.71 | $^{141}_{58}$Ce | 198.8 | | 58.4 |
| $^{142}_{58}$Ce | 33.5 | 28±1 | 16.7 | | | | |
| $^{141}_{59}$**Pr** | 101 | 111.4±1.4 | 130 | $^{142}_{59}$Pr | 233 | | 261 |
| $^{143}_{59}$Pr | 170 | | 57.7 | | | | |
| $^{142}_{60}$**Nd** | 54.5 | 35.0±0.7 | 22.9 | $^{143}_{60}$Nd | 362.4 | 245±3 | 105 |
| $^{144}_{60}$Nd | 82.3 | 81.3±1.5 | 37.1 | $^{145}_{60}$Nd | 617.9 | 425±5 | 207 |
| $^{146}_{60}$Nd | 128.7 | 91.2±1.0 | 56.8 | $^{147}_{60}$Nd | 1434.4 | | 663 |
| $^{147}_{61}$Pm | 1210.4 | 709±100 | 452 | $^{148}_{61}$Pm | 1529.7 | | |
| $^{144}_{62}$**Sm** | 91.0 | 92± 6 | 38.6 | $^{147}_{62}$Sm | 1229 | 973±10 | 584 |
| $^{148}_{62}$Sm | 340 | 241±2 | 130 | $^{149}_{62}$Sm | 1622 | 1820±17 | 1274 |

MOST results in almost all cases. In the next part of the discussion, we comment only on the more significant results.

The Cs isotopes that are involved in the s-process are $^{133,134,135}$Cs. The nucleus $^{134}$Cs is unstable with a half life of 2.06 years and no neutron capture data is yet available. However, this is an important for the abundance of $^{134,136}$Ba in view of the strong branching at $^{134}$Cs. The compilation by Bao *et al.* [41] recommended a MACS value of 664±174 mb. Our calculated value for $^{135}$Cs is close to the experimental measurements. However, the neutron deficient $^{133}$Cs rate is comparatively poorly reproduced.

Dillmann *et al.* [3] have measured the MACS for a number of nuclei relevant to p-process. The measured values at $kT = 25$ keV for the nuclei $^{130,132}$Ba are 736±29 mb and 392.6±14.8 mb, respectively. Our calculated value for $^{130,132}$Ba at 25 keV are 675.3 and 424.1 mb, respectively. The neutron capture cross-sections of the s-only nuclei $^{134,136}$Ba are very important for constraining the s-process. The cross-section for $^{136}$Ba is also known to be an important ingredient in determining the mean neutron exposure in the main s-process component. As one can see, here also our results are reasonably close to experimental measurements except in the case of $^{130}$Ba.

Käppeler *et al.* measured the cross-sections for stable Ce isotopes [44]. They then constructed an optical model potential for this region and calculated the cross-sections for $^{141}$La and $^{142,143}$Pr in the Hauser-Feshbach formalism. Their calculated values for these two nuclei at 30 keV are 91 mb, 297 mb, and 205 mb, respectively. Although their results for $^{140,142}$Ce and $^{141}$Pr are very close to our calculations, the value for $^{141}$Ce is smaller by more than a factor of two while that for $^{142,143}$Pr is larger by more than 25% and 20%, respectively. The results for La and Pr isotopes are also close to experimental measurements. The nucleus $^{138}$La is produced in the p-process. However, results for more neutron deficient Ce isotopes do not agree well with experiments.

As one goes to heavier isotopes, agreement becomes poorer except in a few cases such as $^{144}$Nd and $^{144}$Sm, though they are still better than the MOST calculation. In general, the poor agreements may be due to the fact

TABLE III: Maxwellian averaged neutron capture cross-sections of $^{138}$Ba, $^{139}$La, $^{140}$Ce, $^{141}$Pr, and $^{142}$Nd. The experimental values presented are from Ref. [40]. See text for more details about the experiments and the available latest measurements not included in Ref. [40].

| $kT$(MeV) | MACS (mb) | | | | | | | | | |
|---|---|---|---|---|---|---|---|---|---|---|
| | $^{138}$Ba | | $^{139}$La | | $^{140}$Ce | | $^{141}$Pr | | $^{142}$Nd | |
| | Pres. | Expt. | Pres. | Expt. | Pres. | Expt. | Pres. | Expt. | Pres. | Expt. |
| 0.005 | 10.3 | 13.4 | 118 | 111.2 | 34.0 | 23 | 353 | 412 | 146.5 | 98.6 |
| 0.010 | 6.96 | 7.85 | 68.9 | 63.2 | 21.9 | 19.5 | 215 | 247 | 95.8 | 65.1 |
| 0.015 | 5.68 | 5.93 | 50.8 | 48.1 | 17.6 | 16 | 161 | 182 | 76.2 | 51.3 |
| 0.020 | 4.93 | 4.95 | 41.2 | 40.3 | 15.2 | 13.5 | 132 | 148 | 65.8 | 43.4 |
| 0.025 | 4.46 | 4.38 | 35.2 | 35.7 | 13.8 | 12 | 114 | 126 | 58.8 | 38.4 |
| 0.030 | 4.14 | 4.00 | 31.0 | 32.4 | 12.7 | 11.0 | 101 | 111 | 54.5 | 35.0 |
| 0.040 | 3.61 | 3.49 | 25.4 | 27.7 | 11.2 | 9.5 | 82.8 | 91.5 | 47.9 | 30.7 |
| 0.050 | 3.28 | 3.14 | 21.8 | 23.6 | 10.2 | 8.7 | 70.8 | 78.3 | 43.8 | 27.7 |
| 0.060 | 3.08 | 2.89 | 19.2 | 22.0 | 9.5 | 8.1 | 62.0 | 69.0 | 41.0 | 25.5 |
| 0.080 | 2.76 | 2.52 | 15.8 | 18.4 | 8.6 | 7.2 | 50.1 | 56.2 | 37.4 | 22.9 |
| 0.100 | 2.58 | 2.23 | 13.7 | 15.2 | 8.0 | 6.6 | 42.4 | 47.6 | 35.5 | 21.0 |

that away from the closed shell, deformation effects come into the picture. However, our calculation is unable to explain the recent results for $^{142}$Nd, a spherical nucleus with $N = 82$, though some of the older measurements for $^{142}$Nd are closer to our calculation. Results for all the other nuclei with $N = 82$ are explained with a good accuracy.

As already pointed out, modern measurements have emphasized the importance of the MACS values at various thermal energies. Hence a number of works, apart from the already mentioned, have measured the MACS values at different temperatures. We present the MACS values at different temperatures for $N = 82$ isotopes in Table III and draw attention to some important results. Heil *et al.* [45] have used neutron activation studies to measure the MACS value at 5.1 keV as $13.0 \pm 0.5$ mb in $^{138}$Ba. In the present work, MACS for $^{138}$Ba is calculated to be 10.2 mb at $kT = 5.1$ keV.

Natural lanthanum is nearly mono-isotopic. It is an important element as it can be easily detected in solar spectroscopy. It is produced in both s- and r-processes and is particularly suitable for monitoring s-process abundances from Ba to Pb. This has led to the study of $^{139}$La through neutron TOF spectroscopy as well as activation measurement. In Table III, we present the MACS values at different temperatures. O'Brien *et al.* have measured the Maxwellian averaged cross-section (MACS) at $kT = 30$ keV as 31.6±0.6 mb [46]. Our calculated value of 31.0 mb agrees with the measurements. Activation technique has also been used to measure MACS at $kT = 5$ keV. The measured value 113.7±4.0 [47] is in excellent agreement with our calculation. Terlizzi *et al.* have measured the resonance parameters in the energy range 0.6 eV to 9 eV and have recalculated the MACS values in the light of their measurements [48]. Their values also lie close to our calculated results. For example, their measurement yields a value of 106.9±5.3 mb at $kT = 5$ keV after normalization to the value for 25 keV from Ref. [46].

Käppeler *et al.* [44] also used the $^7$Li$(p, n)^7$Be reaction to study the thermal neutron capture by Ce isotopes at 25 keV. They obtained a MACS value of 12.0±0.4 mb. This was extrapolated to other thermal energy values. As already mentioned, Voss *et al.* [27] have obtained the MACS values as a function of temperature for $^{141}$Pr.

As already mentioned, Wisshak *et al.* [33] studied the neutron capture cross sections of Nd isotopes. They have also calculated the MACS values at different energy from their data. Guber *et al.* [49] also measured the MACS values between $kT = 5$ - 50 keV. Both the above references have commented on the importance of the new measurements in s-process.

## IV. SUMMARY

To summarize, astrophysically important neutron capture reactions near the $N = 82$ shell closure have been

studied using a microscopic approach. Densities of relevant nuclei near have been calculated in the RMF approach. The calculated charge densities and radii agree with experimental measurements, whenever available. The calculated density has been folded with DDM3Y nucleon-nucleon interaction to obtain the optical model potential for neutron reactions. Cross sections for $(n, \gamma)$ reactions have been calculated and compared with measurements. Finally Maxwellian average cross-section values, important for s- and p-processes, have been calculated.

### Acknowledgment

The authors acknowledge the financial support provided by University Grants Commission (India), Department of Science and Technology, Alexander Von Humboldt Foundation, and the University of Calcutta.

[1] M. E. Burbidge, G. R. Burbidge, W. A. Fowler, and F. Hoyle, Rev. Mod. Phys. **29**, 547 (1957).
[2] F. Käppeler, R. Gallino, S. Bisterzo, and W. Aoki, Rev. Mod. Phys. **83**, 157 (2011).
[3] I. Dillmann, C. Domingo-Pardo, M. Heil, F. Käppeler, S. Walter, S. Dababneh, T. Rauscher, and F.-K. Thielemann, Phys. Rev. C **81**, 015801 (2010).
[4] G. Gangopadhyay, Phys. Rev. C **82**, 027603 (2010)
[5] C. Lahiri and G. Gangopadhyay, Eur. Phys. J. A **47**, 87 (2011)
[6] C. Lahiri and G. Gangopadhyay, Phys. Rev. C **84**, 057601 (2011)
[7] C. Lahiri and G. Gangopadhyay, Phys. Rev. C **86**, 047601 (2012)
[8] S. Dutta, D. Chakraborty, G. Gangopadhyay, and A. Bhattacharyya, Phys. Rev. C **91**, 025804 (2015)
[9] D. Chakraborty, S. Dutta, G. Gangopadhyay, and A. Bhattacharyya, Phys. Rev. C **91**, 057602 (2015).
[10] B. G. Todd-Rutel and J. Piekarewicz, Phys. Rev. Lett. **95**, 122501 (2005).
[11] A. Bouyssy, J. F. Mathiot, and N. Van Giai, and S. Marcos, Phys. Rev. C **36**, 380 (1987).
[12] G. Bertsch, J. Borysowicz, H. McManus, and W.G. Love, Nucl. Phys. **A 284**, 319 (1977).
[13] G. R. Satchler and W. G. Love, Phys. Rep. **55**, 183 (1979).
[14] W. D. Myers, Nucl. Phys. **A 204**, 465 (1973).
[15] D. N. Basu, J. Phys. G: Nucl. Part. Phys. **30**, B7(2004).
[16] R. R. Scheerbaum, Nucl. Phys. **A 257**, 77(1976)
[17] A. J. Koning, S. Hilaire, and M. Duizvestijn, in *Proceedings of the International Conference on Nuclear Data for Science and Technology, April 2227, 2007, Nice, France*, edited by O. Bersillon, F. Gunsing, E. Bauge, R. Jacqmin, and S. Leray (EDP Sciences, Cedex, France, 2008), p. 211.
[18] S. Goriely, Phys. Lett. **B 436**, 10 (1998)
[19] J. Heisenberg, R. Hofstadter, J. S. McCarthy, I. Sick, M. R. Yearian, B. C. Clark, R. Herman, and D. G. Ravenhall, in *Topics in Modern Physics: Tribute to E.U. Condon* , edited by W.E. Brittin and H. Odabasi (Adam Hilger, London, 1970), p 169.
[20] M. A. Moinester, J. Alster, G. Azuelos, J. B. Bellicard, B. Frois, M. Huet, P. Leconte, and Phan Xuan Ho, Phys. Rev. C **24**, 80 (1981).
[21] I. Angeli, At. Data Nucl. Data Tables **87**, 185 (2004).
[22] R. L. Macklin, Nucl. Sci. Eng. **81**, 418 (1982)
[23] N. Yamamuro, M. Igashira, T. Sekiya, and H. Shirayanagi, J. Nucl. Sci. Technol. (Tokyo) **20**, 797 (1983).
[24] J. Voignier, S. Joly, G. Grenier, Nucl. Sci. Eng. **112**, 87 (1992)
[25] M. Igashira, M. Saito, J. Nishiyama, T. Ohsaki, and T. Katabuchi, Proc. Intern. Conf. Nuclear Data for Science and Technology,
[26] S. Harnood, M. Igashira, T. Matsumoto, S. Mizuno, and T. Ohsaki, J. Nucl. Sci. Technol. (Tokyo) **37**, 740 (2000).
[27] F. Voss, K. Wisshak, C. Arlandini, F. Käppeler, L. Kazakov, and T. Rauscher, Phys. Rev. C **59**, 1154 (1999).
[28] J. Voignier, S. Joly, and G.Grenier, Nucl. Sci. Eng. **112**, 87 (1992). Nice, France, April 22-27, 2007, O. Bersillon, F. Gunsing, E. Bauge, R. Jacqmin, and S. Leray, Eds., p.1299 (2008); EDP Sciences, 2008
[29] F. Voss, K. Wisshak, K. Guber, F. Käppeler, and G. Reffo, Phys. Rev. C **50**, 2582 (1994).
[30] F. Voss, K. Wisshak, and F. Käppeler, Phys. Rev. C **52**, 1102 (1995).
[31] H. Beer, F. Corvi, and P. Mutti, Astro. J. **474**, 843 (1997).
[32] H. Beer and F. Käppeler, Phys. Rev. C **21**, 534 (1980).
[33] K. Wisshak, F. Voss, F. Käppeler, L. Kazakov, and G. Reffo, Phys. Rev. C **57**, 391 (1998).
[34] K. Wisshak, F. Voss, F. Käppeler, Phys. Rev. C **57**, 3452 (1998).
[35] T. Veerapaspong, M. Igashira, S. Mizuno, J. Hori, and T. Ohsaki, J. Nucl. Sci. Technol. (Tokyo) **36**, 855 (1999).
[36] R. L. Macklin, N. W. Hill, J. A. Harvey, and G. L. Tweed, Phys. Rev. C **48**, 1120 (1993).
[37] K. Wisshak, K. Guber, F. Voss, F. Käppeler, and G. Reffo, Phys. Rev. **C 48**, 1401 (1993).
[38] M. Mizumoto, Nucl. Phys. **A 357**, 90 (1981).
[39] B. Diamet. M. Igashira, M. Mizumachi, S. Miziuno, J.

Hori, K. Masuda and T. Ohsaki, J. Nucl. Sci. Technol. (Tokyo) **36**, 865 (1999).
[40] I. Dillmann, R. Plag, F. Käppeler, T. Rauscher, KADoNiS v0.3 - The third update of the "Karlsruhe Astrophysical Database of Nucleosynthesis in Stars" in *EFNUDAT Fast Neutrons, Proceedings of the Scientific Workshop on Neutron Measurements, Theory and Applications* 28 - 30 April, 2009, Geel, Belgium, edited by F. -J. Hambsch (Publications Office of the European Union, Luxembourg, 2010) p. 55 ; http://kadonis.org.
[41] Z. Y. Bao, H. Beer, Käppeler, F. Voss, and K. Wisshak, Atom. Data. Nucl. Data Tables **76**, 70 (2000).
[42] S. Goriely, Phys. Lett. **B 436**, 10 (1998).
[43] M. Arnould and S. Goriely, Phys. Rep. **384**, 1 (2003).
[44] F. Käppeler, K. A. Toukan, M. Schumann, and A. Mengoni, Phys. Rev. C **53**, 1397 (1996).
[45] M. Heil, S. Dababneh, A. Juseviciute, F. Käppeler, R. Plag, R. Reifarth, and S. OBrien, Phys. Rev. C **71**, 025803 (2005)
[46] S. O'Brien, S. Dababneh, M. Heil, F. Käppeler, R. Plag, R. Reifarth, R. Gallino, and M. Pignatari, Phys. Rev. C **68**, 035801 (2003).
[47] N. Winckler, S. Dababneh, M. Heil, F. Käppeler, R. Gallino, and M. Pignatari, Astr. J. **647**, 685 (2006).
[48] R. Terlizzi *et al.* , Phys. Rev. C **75**, 035807 (2007).
[49] K. H. Guber, R. R. Spencer, P. E. Koehler and R. R. Winters, Phys. Rev. Lett. **78**, 2704 (1997).